

Racah materials: role of atomic multiplets in intermediate valence systems

A. B. Shick,¹ L. Havela,² A. I. Lichtenstein,^{3,4} and M. I. Katsnelson^{5,4}

¹*Institute of Physics, ASCR, Na Slovance 2, CZ-18221 Prague, Czech Republic*

²*Department of Condensed Matter Physics, Charles University,
Ke Karlovu 5, CZ-12116, Prague, Czech Republic*

³*University of Hamburg, Jungiusstrasse 9, 20355 Hamburg, Germany*

⁴*Theoretical Physics and Applied Mathematics Department,*

Ural Federal University, Mira Str.19, 620002, Ekaterinburg, Russia

⁵*Radboud University Nijmegen, Heyendaalseweg 135, 6525 AJ Nijmegen, The Netherlands*

(Dated: July 26, 2021)

We address the long-standing mystery of the nonmagnetic insulating state of the intermediate valence compound SmB_6 . Within a combination of the local density approximation (LDA) and an exact diagonalization (ED) of an effective discrete Anderson impurity model, the intermediate valence ground state with the f -shell occupation $\langle n_{4f} \rangle = 5.6$ is found for the Sm atom in SmB_6 . This ground state is a singlet, and the first excited triplet state ~ 3 meV higher in the energy. SmB_6 is a narrow band insulator already in LDA, with the direct band gap of ~ 10 meV. The electron correlations increase the band gap which now becomes indirect. Thus, the many-body effects are relevant to form the indirect band gap, crucial for the idea of “topological Kondo insulator” in SmB_6 . Also, an actinide analog PuB_6 is considered, and the intermediate valence singlet ground state is found for the Pu atom. We propose that $[\text{Sm}, \text{Pu}]\text{B}_6$ belong to a new class of the intermediate valence materials with the multi-orbital “Kondo-like” singlet ground-state. Crucial role of complex spin-orbital f^n - f^{n+1} multiplet structure differently hybridized with ligand states in such Racah materials is discussed.

PACS numbers: 71.28.+d, 71.20.-b

Valence fluctuations in the f -electron based materials near the localization threshold attract significant attention in the condensed matter physics. The intermediate valence has been considered originally to describe some of the rare-earth compounds with Ce, Sm, Eu, Tm, and Yb elements. The original idea was that the single-particle “promotion energy” from $4f$ to $5d$ states changes the sign in these systems [1, 2]. Soon, it was realized that the situation is different for the special case of Ce. In mixed-valence Ce compounds there is a partial delocalization of $4f$ electrons due to direct overlap of their wave functions ($4f$ band formation), rather than their promotion to $5d$ band [3]. Later it was suggested that similar physics is relevant for $5f$ electrons in Pu [4].

A careful examination of various intermediate valence systems uncovers many differences between them. At first, what are the properties of competing configurations? For Ce, this is f^0 and f^1 ; for Yb (like in YbB_{12} [2] or elemental Yb under pressure [5]) this is f^{13} and f^{14} . In both these cases one of those configurations is trivial in a many-body sense (completely empty or completely occupied $4f$ shell). For Sm the competing configurations are f^5 and f^6 , and for Eu - f^6 and f^7 . In this situation, the atomic f^n spin-orbital coupling (SOC) and term effects are essential. Rather than to assume the promotion between single-particle f - and d -states, one needs to consider the competition of ground-state multiplets corresponding to those configurations. Roughly speaking, this is the case when the Hubbard bands originated from these multiplets are well separated. Namely, one of the sub-bands has a well-pronounced multiplet structure in solids, and for another part of the spectrum, the multiplets are merged into a single quasiparticle sub-band [6]. This picture bears close similarities to the case of δ -Pu, which was called “*Racah metal*” [7].

Here we apply this concept to another $4f$ and $5f$ systems, using SmB_6 and PuB_6 as examples of the “*Racah materials*”. Recently, these materials were proposed as candidates to 3D topological insulators [8–10], as well as ytterbium borides [11]. We primarily focus not on the topological properties of electronic bands in SmB_6 and PuB_6 , but on the physics of valence fluctuations and multiplet transitions in these systems. The formation of mixed valence singlet non-magnetic states in effective Anderson impurity model for these compounds crucially depends on hybridization parameters with the ligand bath orbitals and is not the universal property of such “Kondo insulators”. Empirically, all known mixed valence Sm and Eu compounds are nonmagnetic, similar to Yb mixed-valence compounds and contrary to Tm ones [1, 2]; the case of Tm is special in a sense that the ground-state multiplets for both competing configurations, f^{12} and f^{13} are magnetic. One can speculate that there is a general reason that mixed valence systems cannot be magnetically ordered if one of the competing

ground states are nonmagnetic. We show that this is, rather, a “play of numbers”; and requires the optimal hybridisation strength. In particular, we have demonstrated that a typical energy of magnetic excitations is an order of magnitude smaller than a typical energy of valence fluctuations.

Although PuB₆ has lately attracted the theoretical attention, very little is known about its properties. The CaB₆ structure type corresponds to the cubic CsCl-type lattice in which the B₆ octahedra occupy the Cl site. In this structure, the B₆ octahedra are linked together in all six orthogonal directions and the Pu-Pu contact distance of 4.11 Å is essentially non-bonding. The paper [12] mentions only a weak temperature dependence of magnetic susceptibility. This would suggest that the 5*f* occupancy should be at least 5.2 or higher, as Pu systems with lower 5*f* count are known to be magnetic [13]. It is interesting that the suggestion that PuB₆ has a valency lower than 3+ appeared already in the work of Smith and Fisk [12] on the basis of volume and color and that the Kondo effect was considered to be responsible for the lack of magnetic moments. SmB₆ belongs to canonical valence fluctuation materials (valence estimated as 2.5-2.6) with the Fermi level in a hybridization gap [14]. Careful photoemission experiments [15–17] clearly support the complicated mixed valence nature of this “topological insulator”.

Our aim is to apply the state-of-the-art many-body method to develop a complete quantitative theory of electronic structure in SmB₆ and PuB₆. We follow the “LDA++” methodology [18], and consider the multi-band Hubbard Hamiltonian $H = H^0 + H^{\text{int}}$, $H^0 = \sum_{i,j,\gamma} H_{i\gamma_1,j\gamma_2}^0 c_{i\gamma_1}^\dagger c_{j\gamma_2}$, where i, j label lattice sites and $\gamma = (lm\sigma)$ mark spinorbitals $\{\phi_\gamma\}$, is the one-particle Hamiltonian found from *ab initio* electronic structure calculations of a periodic crystal; H^{int} is the on-site Coulomb interaction [18] describing the *f*-electron correlation. The effects of the interaction Hamiltonian H^{int} on the electronic structure are described by a \mathbf{k} -independent one-particle self energy, $\Sigma(z)$ (where z is a (complex) energy), which is constructed with the aid of an auxiliary impurity model describing the complete seven-orbital 5*f* shell. This multi-orbital impurity model includes the full spherically symmetric Coulomb interaction, the spin-orbit coupling (SOC), and the crystal field (CF). The corresponding Hamiltonian can be written as [19]

$$\begin{aligned} H_{\text{imp}} = & \sum_{kmm'\sigma\sigma'} [\epsilon^k]_{mm'}^{\sigma\sigma'} b_{km\sigma}^\dagger b_{km'\sigma'} + \sum_{m\sigma} \epsilon_f f_{m\sigma}^\dagger f_{m\sigma} \\ & + \sum_{mm'\sigma\sigma'} [\xi \mathbf{l} \cdot \mathbf{s} + \Delta_{\text{CF}}]_{mm'}^{\sigma\sigma'} f_{m\sigma}^\dagger f_{m'\sigma'} \\ & + \sum_{kmm'\sigma\sigma'} \left([V^k]_{mm'}^{\sigma\sigma'} f_{m\sigma}^\dagger b_{km'\sigma'} + h.c. \right) \\ & + \frac{1}{2} \sum_{mm'm''m'''\sigma\sigma'} U_{mm'm''m'''} f_{m\sigma}^\dagger f_{m'\sigma'}^\dagger f_{m''\sigma''} f_{m'''\sigma'''} \end{aligned} \quad (1)$$

where $f_{m\sigma}^\dagger$ creates an electron in the 5*f* shell and $b_{km\sigma}^\dagger$ creates an electron in the “bath” that consists of those host-band states that hybridize with the impurity 5*f* shell. The energy position ϵ_f of the impurity level, and the bath energies ϵ^k are measured from the chemical potential μ . The parameters ξ and Δ_{CF} specify the strength of the SOC and the magnitude of the crystal field (CF) at the impurity. The parameter matrices V^k describe the hybridization between the *f* states and the bath orbitals at energy ϵ^k .

The band Lanczos method [20] is employed to find the lowest-lying eigenstates of the many-body Hamiltonian H_{imp} and to calculate the one-particle Green’s function $[G_{\text{imp}}(z)]_{mm'}^{\sigma\sigma'}$ in the subspace of the *f* orbitals at low temperature ($k_B T = 1/500$ eV). The selfenergy $[\Sigma(z)]_{mm'}^{\sigma\sigma'}$ is then obtained from the inverse of the Green’s function matrix $[G_{\text{imp}}]$.

Once the selfenergy is known, the local Green’s function $G(z)$ for the electrons in the solid,

$$[G(z)]_{\gamma_1\gamma_2} = \frac{1}{V_{\text{BZ}}} \int_{\text{BZ}} d^3k [z + \mu - H_{\text{LDA}}(\mathbf{k}) - \Sigma(z)]_{\gamma_1\gamma_2}^{-1}, \quad (2)$$

is calculated in a single-site approximation as given in [21]. Then, with the aid of the local Green’s function $G(z)$, we evaluate the occupation matrix $n_{\gamma_1\gamma_2} = -\frac{1}{\pi} \text{Im} \int_{-\infty}^{E_F} dz [G(z)]_{\gamma_1\gamma_2}$. The matrix $n_{\gamma_1\gamma_2}$ is used to construct an effective LDA+*U* potential V_U , which is inserted into Kohn–Sham-like equations:

$$[-\nabla^2 + V_{\text{LDA}}(\mathbf{r}) + V_U + \xi(\mathbf{l} \cdot \mathbf{s})] \Phi_{\mathbf{k}}^b(\mathbf{r}) = \epsilon_{\mathbf{k}}^b \Phi_{\mathbf{k}}^b(\mathbf{r}). \quad (3)$$

These equations are iteratively solved until self-consistency over the charge density is reached. In each iteration, a new Green’s function $G_{\text{LDA}}(z)$ (which corresponds to $G(z)$ from Eq.(2) with the self energy Σ set to zero), and a new value of the 5*f*-shell occupation are obtained from the solution of Eq. (3). Subsequently, a new self energy $\Sigma(z)$ corresponding to the updated *f*-shell occupation is constructed. Finally, the next iteration is started by evaluating the new local Green’s function, Eq.(2).

SmB₆ and PuB₆ crystallize in the CaB₆-structure with the space group $Pn3m$ (221), as shown in Fig. S1 (supplementary information). The experimental lattice constants of 4.1333 Å for SmB₆ and 4.1132 Å for PuB₆ are used. In the calculations we used an in-house implementation [22, 23] of the FP-LAPW method that includes both scalar-relativistic and spin-orbit coupling effects. For SmB₆, the Slater integrals were chosen as $F_0 = 6.87$ eV, and $F_2 = 9.06$ eV, $F_4 = 6.05$ eV, and $F_6 = 4.48$ eV [24]. They corresponds to commonly accepted values for Coulomb $U = 6.87$ eV and Hund exchange $J = 0.76$ eV, and are in the ballpark of the parameters commonly used in the calculations of the rare-earth materials [25]. For PuB₆, the Slater integrals $F_0 = 4.0$ eV, and $F_2 = 7.76$ eV, $F_4 = 5.05$ eV, and $F_6 = 3.07$ eV were chosen [26]. They corresponds to commonly accepted values for Coulomb $U = 4.0$ eV and exchange $J = 0.64$ eV. The SOC parameters $\xi = 0.16$ eV for SmB₆, and 0.29 eV for PuB₆ were determined from LDA calculations. CF effects were neglected and Δ_{CF} was set to zero. For the double-counting term entering the definition of the LDA+ U potential, V_U , we have adopted the fully-localized (or atomic-like) limit (FLL) $V_{dc} = U(n_f - 1/2) - J(n_f - 1)/2$. Furthermore, we set the radii of the atomic spheres to 2.85 a.u. (Sm), 3.0 a.u. (Pu), 1.53 a.u. (B). The parameter $R_{Sm} \times K_{max} = 9.98$ determined the basis set size, and the Brillouin zone (BZ) sampling was performed with 1331 k points. The self-consistent procedure defined by Eqs. 1–3 was repeated until the convergence of the f -manifold occupation n_f was better than 0.01.

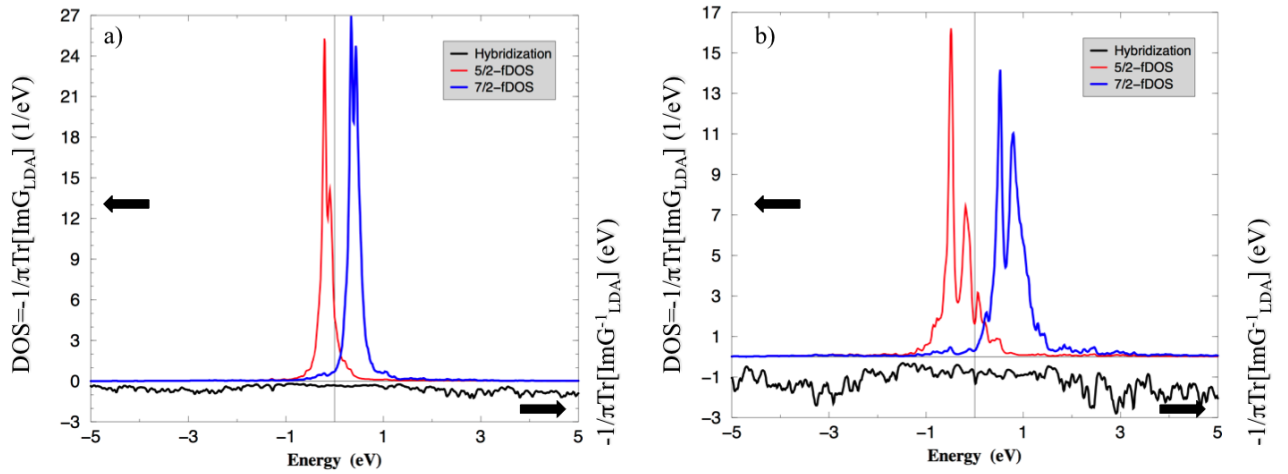


FIG. 1: LDA $j = 5/2, 7/2$ projected DOS, and LDA hybridization function $\frac{\Delta(\epsilon)}{\pi} = -\frac{1}{\pi} \text{ImTr}[G^{-1}(\epsilon + i\delta)]$ for SmB₆ (a) and PuB₆(b) .

In order to determine the bath parameters V^k and ϵ^k , we assume that the LDA represents the non-interacting model. We then associate the LDA Green's function $G_{\text{LDA}}(z)$ with the Hamiltonian of Eq. (1) when the coefficients of the Coulomb interaction matrix are set to zero ($U_{mm'm''m'''} = 0$). The hybridization function $\Delta(\epsilon)$ is then estimated as $\Delta(\epsilon) = -\text{ImTr}[G_{\text{LDA}}^{-1}(\epsilon + i\delta)]$. The curve obtained for $\frac{1}{\pi}\Delta(\epsilon)$ is shown in Fig. 1, together with the LDA density of states (total and $j = 5/2, 7/2$ -projected). The results show that the hybridization matrix is, to a good approximation, diagonal in the $\{j, j_z\}$ representation. Thus, we assume the first and fourth terms in the impurity model, Eq. (1), to be diagonal in $\{j, j_z\}$, so that we only need to specify one bath state (six orbitals) with $\epsilon_{j=5/2}^{k=1}$ and $V_{j=5/2}^{k=1}$, and another bath state (eight orbitals) with $\epsilon_{j=7/2}^{k=1}$ and $V_{j=7/2}^{k=1}$. Assuming that the most important hybridization is the one occurring in the vicinity of E_F , as suggested by the curve shown in Fig. 1, the numerical values of the bath parameters $V_{5/2,7/2}^{k=1}$ are found from the relation [27] $\pi \sum_k |V_k^j|^2 \delta(\epsilon_k^j - \epsilon) = -\Delta(\epsilon)/N_f$ averaged over the energy interval, $E_F - 0.5$ eV $\leq \epsilon \leq E_F + 0.5$ eV, with $N_f = 6$ for $j = 5/2$ and $N_f = 8$ for $j = 7/2$. The bath-state energies $\epsilon_{5/2,7/2}^{k=1}$ shown in Table I are adjusted to approximately reproduce the LDA f -states occupations $n_f^{5/2}$ and $n_f^{7/2}$.

The magnitude of $\Delta(E_F) (\equiv \Delta_v)$ is a characteristic energy of the valence fluctuations, in a sense that for the time scale $t > \frac{\hbar}{\Delta_v} \equiv \tau_{fl}$ the system behaves as a homogeneous with the physical properties which are intermediate between those for Sm²⁺ and Sm³⁺ whereas for $t < \tau_{fl}$ it is a random configuration of "frozen" Sm²⁺ and Sm³⁺ ions [1, 2, 5]. Lattice parameter and core-level X-ray spectra serve as examples of the properties of the first and the second kind.

TABLE I: f -states occupations $n_f^{5/2}$ and $n_f^{7/2}$, and bath state parameters $\epsilon_{5/2,7/2}^1$ (eV), $V_{5/2,7/2}^1$ (eV) for Sm and Pu-atoms in SmB_6 , and PuB_6 from LDA calculations.

Material	$n_f^{5/2}$	$n_f^{7/2}$	$\epsilon_1^{5/2}$	$V_1^{5/2}$	$\epsilon_1^{7/2}$	$V_1^{7/2}$
SmB_6	5.28	0.26	-0.20	0.16	0.07	0.15
PuB_6	4.89	0.40	0.13	0.26	-0.05	0.17

SmB₆

First, we focus on SmB_6 , and discuss the solution of Eq.(1). The ground state of the cluster formed by the $4f$ shell and the bath is given by a non-magnetic singlet with all angular moments of the $5f$ -bath cluster equal to zero ($S = L = J = 0$). For the $4f$ shell alone, the $\langle n_f \rangle = 5.63$, and the $\langle n_{\text{bath}} \rangle = 6.37$ bath states. Note that $\langle n_f \rangle$ slightly exceeds its LDA value of 5.54. The expectation values of the spin S_f , orbital L_f and total J_f angular moments can be calculated as $\langle \hat{X}_f^2 \rangle = X_f(X_f + 1)$ ($X_f = S_f, L_f, J_f$), giving $S_f = 2.77$, $L_f = 3.80$, and $J_f = 1.88$. The ground state is separated from the first excited state by the gap $\Delta_m = 2.6$ meV. Surprisingly, this value is in a very good agreement with the experimental activation gap value of 3 meV [28]. This gap should show itself in the magnetic susceptibility, which is anticipated to behave as $1/[T + T_m]$ at high temperatures, with saturation below T_m temperature $\sim \Delta_m$, in qualitative agreement with the experimental data [14], and other experiments which measure the two-particle excitations. This excitation in two-particle spectrum can be contrasted with first single-particle photoemission peak around 20 meV [15]. It is important to mention that formation of mixed-valence multi-orbital singlet in effective Anderson model is very sensitive to hybridization parameters (Table I) and with relative small changes the magnetic ground states is formed in ED calculations. It is also important that this magnetic exciton energy is an order of magnitude smaller than the energy of the valence fluctuations $\Delta_v \approx 70$ meV. This means that the nonmagnetic character of the ground state is not directly related to the valence fluctuations: the system possesses local magnetic moments in the energy (and temperature) range between Δ_m and Δ_v , that is, within the homogeneous intermediate valence regime.

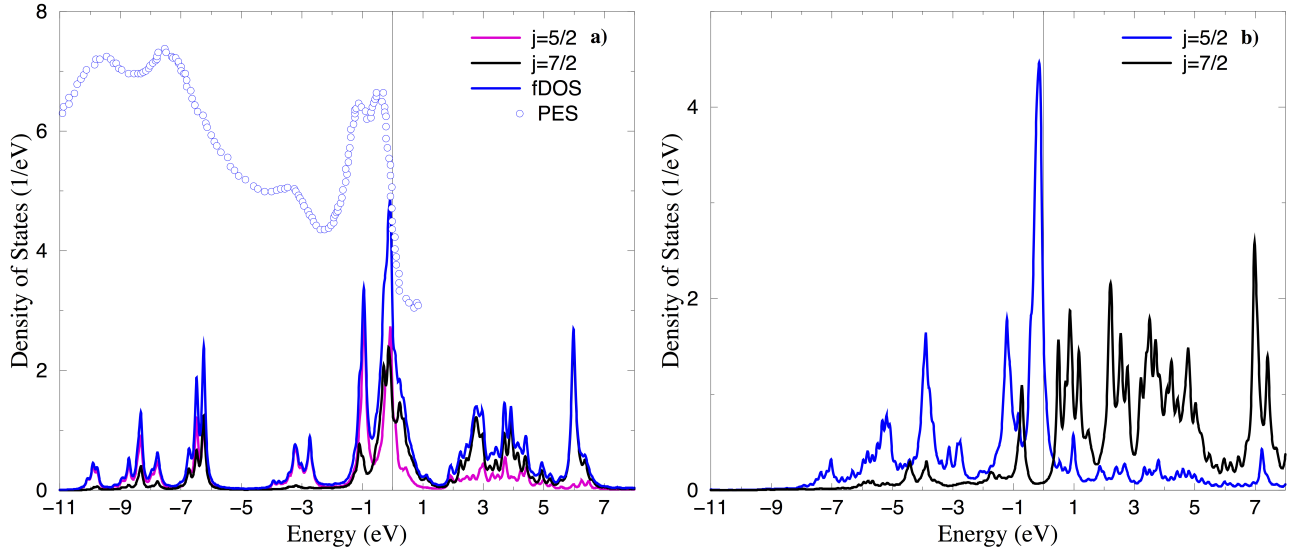


FIG. 2: f -electron density of states (fDOS, and $j = 5/2, 7/2$ projected) for the Sm atom in SmB_6 (a), and the Pu atom in PuB_6 (b). Also comparison with the experimental XPS spectra is given for SmB_6 .

The f -orbital density of states (DOS) obtained from Eq. (2) for SmB_6 is shown in Fig. 2(a). The f -DOS is in agreement with the experimental x-ray photoelectron spectra (XPS) [29], and previously reported Hubbard-I calculations [30]. The many-body resonances near the Fermi energy are produced by $f^6 \rightarrow f^5$ multiplet transitions, they are in a way analogues to the *Racah* peaks, specific transitions between *Racah* multiplets [31] of f^n and $f^{n\pm 1}$.

Fig. S2(a) (supplementary information) shows the LDA band structure together with the band structure calculated from the solutions of Eq. (3), which represents an extended LDA+U band structure with the $5f$ -states occupation matrix obtained from the local impurity Greens function Eq.(2) (LDMA). Note that the LDA band structures are very similar to previously reported results of WIEN2K for SmB_6 [9].

A more detailed look at the band structure is shown in Fig. 3(a) SmB_6 is close to a very narrow band insulator already in LDA. There is a tiny amount of holes in the vicinity of the X-point (similar to Ref. [9]) and a direct gap of ~ 30 meV right above. When the Coulomb interaction is added, it becomes an indirect band insulator with the gap of ~ 60 meV. Note that the band-gap value exceeds somewhat the experimental gap of around 20 meV. Incorporating the dynamical self-energy effects into the LDMA band structure, as described in the supplemental material Fig. S3, we obtain that the indirect band gap is somewhat reduced to ~ 30 meV becoming closer to the experimental value of 20 meV.

It is known that the d - f Coulomb interaction G (Falicov-Kimball interaction) plays a role for the intermediate valence [1, 32, 33]. This interaction leads to the excitonic renormalization of the effective hybridization. The effective hybridization V_{eff} between d and f states with the many-body renormalization can be calculated using the electronic structure expression [32] which for zero temperature reads:

$$V_{eff} \left[1 - \frac{GL_0}{\int d\epsilon N(\epsilon)} \right] = V, \quad L_0 = \int d\epsilon \frac{N(\epsilon)}{(\epsilon^2 + 4V_{eff}^2)^{1/2}}. \quad (4)$$

In this Eq. (4), $N(\epsilon)$ is the total DOS without the f -projected contribution, and V is the LDA hybridization from the Table I. Importantly, the renormalized hybridization turns out to be quite strongly temperature dependent [32].

The parameter G can be determined as the derivative of the center of the $5d$ band with respect to the number n_f of $4f$ electrons [5]). In practice, we have varied n_f by changing the double-counting term from the FLL ($n_f=5.63$) to the “around-mean-field” (AMF, $n_f=5.68$), and obtained the Falicov interaction parameter of 3.8 eV. Solution of the Eq. (4) yields the V_{eff}/V renormalization of 1.77.

Thus, the d - f excitonic effects enhance the hybridization making the hybridization gap larger and therefore favoring the topological insulator behavior. We performed the calculations with this renormalised V_{eff} in Eq. (1), and obtained again the singlet ground state. The $\langle n_f \rangle = 5.61$ has decreased slightly. This numerical stability of the Sm singlet ground state with respect to a hybridization strength is important since experiments [34] show a strong temperature dependence of the energy gap in SmB_6 which cannot be explained in a purely hybridization model; they were explained in Ref. [32] via excitonic effects. Recently, a strong decrease of the hybridization gap with the temperature increase in SmB_6 was found in ARPES [16]. This can be also considered as a confirmation of strong many-body (excitonic) renormalization of the hybridization.

To estimate the temperature dependence of the hybridisation due to Falicov-Kimball interaction we use the theory [32] for the finite temperatures, that is, Eq. (4) with the replacement,

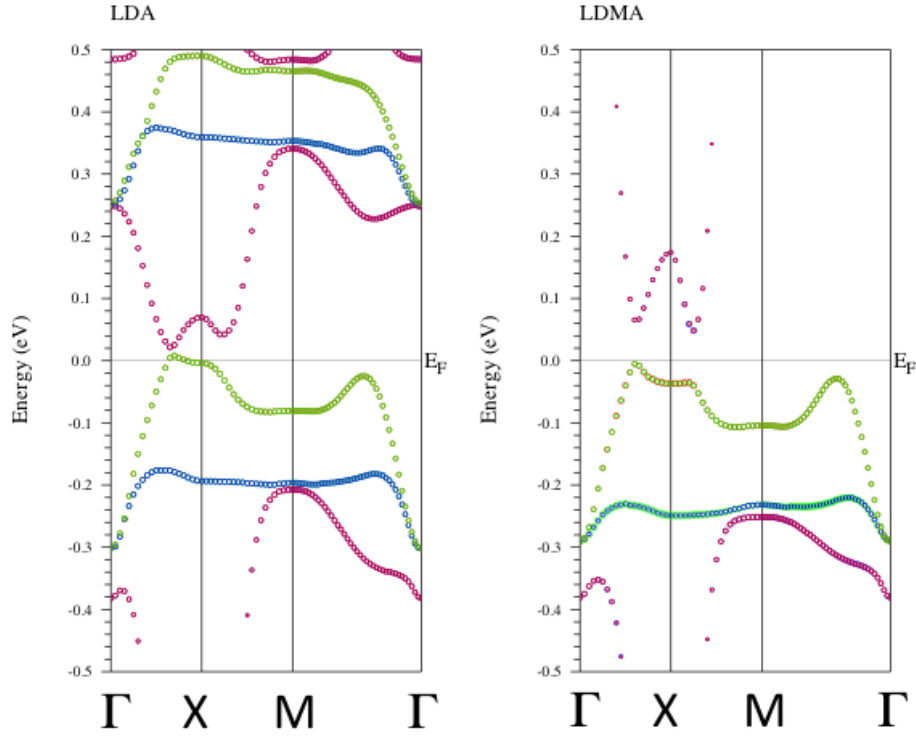
$$L_0 \rightarrow L = \int d\epsilon \frac{N(\epsilon)}{(\epsilon^2 + 4V_{eff}^2)^{1/2}} [1 - f(\epsilon_1) - f(\epsilon_2)], \quad (5)$$

where $\epsilon_{1,2} = \frac{1}{2}((\epsilon^2 + 4V_{eff}^2)^{1/2} \pm \epsilon)$, and $f(\epsilon) = \frac{1}{e^{\epsilon/k_B T} + 1}$ is the Fermi function. The results are shown in Fig. 4.

The presence of the non-magnetic f^6 multiplet is crucially important for the non-magnetic singlet ground state of SmB_6 . For instance, in the intermediate valence TmSe (competition of f^{12} and f^{13} configurations) the ground state is magnetic since both configurations are magnetic. At the same time, there is no “theorem” that for the non-magnetic ground state of one of the competing configurations the system cannot be magnetic, and the specific values of the relevant parameters are important. As we have seen, even typical energy scales for the magnetic (Δ_m) and valence (Δ_v) fluctuations are different.

For the f -shell occupation n_f of 5.6, we show in Fig. 5 the energy difference between the first excited eigenstate for given number of particles ($N = n_{bath} + n_f$) and the ground state of the Eq. 1 for different values of hybridization : those calculated in LDA and given in Tab. I, reduced by a factor of 2, and renormalised by the Falicov-Kimball model, as it was described above. In all those calculations, the ground state is a non-magnetic singlet with $N = 12$. For the LDA hybridization, the lowest excited state belongs to the same $N = 12$, and is lying 3 meV above the ground state. The excited magnetic $N = 11$ and $N = 13$ states are shifted upwards in the energy by 70 meV and 47 meV respectively. When the hybridization is reduced (twice smaller than its LDA value), a non-magnetic ground state singlet with $N = 12$ is by 6 meV lower than almost degenerate $N = 11$ and $N = 12$ magnetic excited states. The $N = 13$ excitation is substantially (by 70 meV) higher in the energy. At

SmB₆



PuB₆

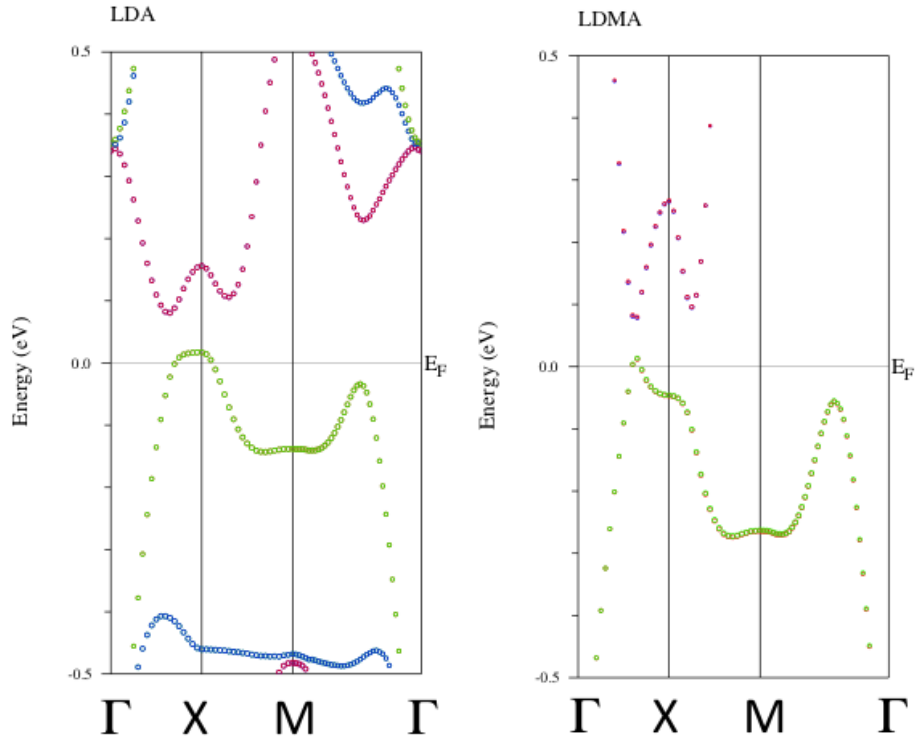


FIG. 3: SmB₆ (a) and PuB₆ (b) LDA and LDMA band structure on the small energy scale. The circles indicate the f-character of the electronic states.

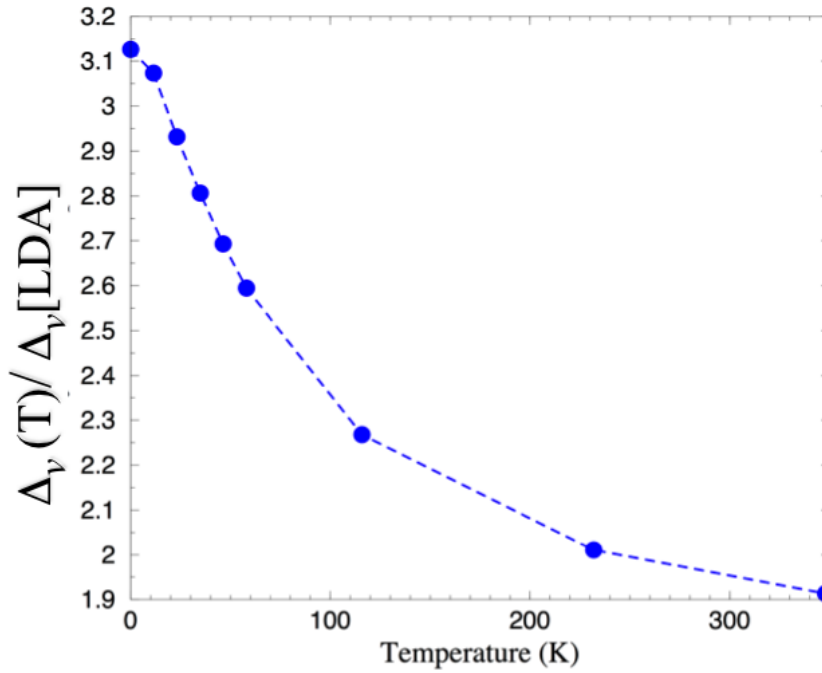


FIG. 4: The temperature dependence of the hybridization gap (indirect), $\Delta_v(T)/\Delta_v[\text{LDA}] = (V_{eff}(T)/V)^2$ calculated in the Falicov-Kimball model Eqs. (4), (5).

the same time, for the hybridization renormalised by the Falicov-Kimball model Eq. 4, the situation is inverse: the lowest magnetic excited state of 4 meV belongs to $N = 13$, next (9 meV) has the same $N = 12$, and the $N = 11$ excitation exceeds the singlet ground state by 139 meV. Further increase of the hybridization, say by a factor of 2 with respect to the LDA value, leads to occurrence of the magnetic $N = 13$ ground state.

In this sense, while it is possible to call the situation “Kondo singlet with high Kondo temperature” (which simply means a formation of singlet from the states of localized and itinerant electrons) one should keep in mind that microscopically some effects beyond the Kondo or Anderson model, such as Falicov-Kimball interactions can contribute significantly. There is an essential difference with various Ce- and Yb-based systems where multiplets are not important, and the situation is indeed closer to the Kondo lattice with high Kondo temperature.

PuB₆

Now we turn to the case of PuB₆. In this case, the hybridization strength is substantially increases (see Table I). The hybridized ground state of the Pu atom in PuB₆, the solution of Eq.(1), is a non-magnetic singlet with all angular moments of the 5*f*-bath cluster equal to zero ($S = L = J = 0$). It consists of $\langle n_f \rangle = 5.49$ *f* states and $\langle n_{bath} \rangle = 8.51$ bath states. As in the case of SmB₆, the magnetic moment of the 5*f* shell ($S_f = 2.23$, $L_f = 3.68$, $J_f = 1.94$) is completely compensated by the moment carried by the electrons in the conduction band. As the value of the 5*f* magnetic moment fluctuates in time, because of the intermediate valence electronic configuration, this compensation must be understood as dynamical in nature. The same situation is realized in δ -Pu ($S_f = 2.11$, $L_f = 4.21$, $J_f = 2.62$), whose ground state is found to be a non-magnetic singlet with $\langle n_f \rangle = 5.21$ and $\langle n_{bath} \rangle = 8.79$ [7].

The *f*-orbital density of states (DOS) obtained from Eq. (2) for PuB₆ is shown in Fig. 2(b). No experimental photoelectron spectra available in this case. As in δ -Pu, there are three many-body resonances near the Fermi energy which are produced by $f^6 \rightarrow f^5$ Racah multiplet transitions.

The LDA band structure is very similar to previously reported results of WIEN2K for PuB₆ [10] as shown in Fig. S2(b) (supplementary information), and, in more details, in Fig. 3(b). Already in the LDA, PuB₆, is close to an insulator with a small amount of holes near the X-point, and the indirect band gap of ~ 60 meV. In the

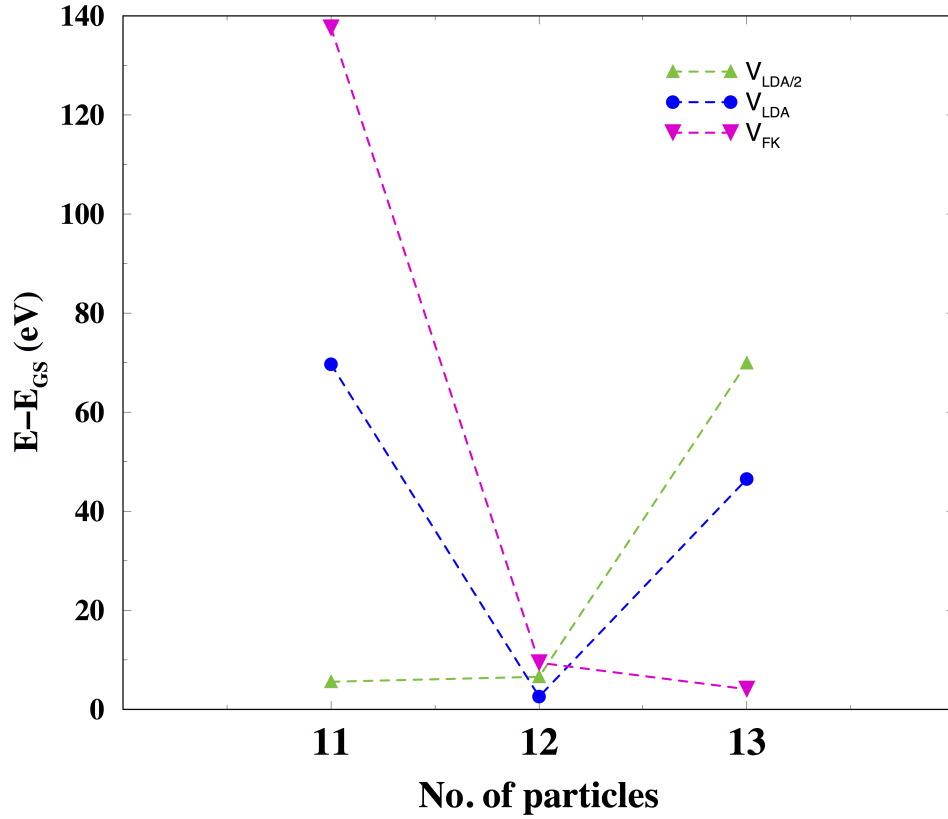


FIG. 5: The energy difference between the first excited eigenstate for given number of particles ($N = n_{bath} + n_f$) and the ground state of the Eq. (1) for different values of hybridization : (i) $V_{LDA/2}$ reduced by a factor of 2 from those calculated in LDA and given in Tab. I, (ii) $V_{LDA/2}$ from Tab. I ; (iii) renormalised by the Falicov-Kimball model Eq. 4.

LDMA, PuB_6 becomes almost an insulator, with the tiny fraction of holes near the X-point, and direct band gap of ~ 60 meV (see Fig. S2(b) and Fig. 3(b)).

As to PuB_6 , we have very little material for comparison with experiment, as there is much less data not only comparing to rare earth borides but also with respect to other Pu compounds. A group of analogous compounds with an energy gap and non-magnetic behaviour are Pu chalcogenides PuX , with $X = \text{S, Se, Te}$. Photoelectron spectra [35, 36] reveal a pronounced fingerprint of the final-state $5f^5$ multiplet close to the Fermi level, which implies that the $5f^6$ state must contribute to the ground state. The Pu chalcogenides have also qualitatively similar non-metallic conductivity explained by hopping [37], qualitatively analogous not only to SmB_6 , but also to Sm chalcogenides.

CONCLUSIONS

The electronic structure calculations are performed within the density functional plus dynamical mean-field theory (“LDA++” [18]) approach combining the local density approximation (LDA) with an exact diagonalization (ED) of the Anderson impurity model for SmB_6 and PuB_6 . The intermediate valence singlet ground states are found for these materials. When the Coulomb $f - f$ (Hubbard) correlations are included, SmB_6 becomes an indirect band gap insulator, while PuB_6 is a direct band gap insulator. A combined effect of specific Racah multiplet structure with intermediate valence behavior of these compounds results in complicated excitation spectrum clearly seen in different photoemission experiments. Formation of singlet ground state in the ED impurity calculations is not universal and crucially depends on structure of two mixed valence multiplets and parameters of effective Anderson model. The Coulomb $f - d$ (Falicov-Kimball) interactions increase essentially

the effective hybridization influencing additionally the singlet state. Their role may be essential in explanation of recently observed temperature-dependent electronic structure of SmB_6 [16]. The calculations illustrate that many-body effects are relevant to form the indirect band gap. In PuB_6 we have found also a mixed-valent singlet ground state with basically the same multiplet physics as was discussed earlier for $\delta\text{-Pu}$ [7].

To emphasize the role of multiplet effects in competing valence states for this class of mixed valence systems, we suggest the term “Racah materials”. The distinguishing feature for these materials is that part of electron excitation spectrum originated from one the valence configurations is more atomic like (with well-pronounced multiplets) whereas for the other valence configuration it is more itinerant-like. The concept of “Racah materials” is somewhat related to the idea of quasiparticle multiplets [38]. Those are represented by atomic-like multiplet transitions $f^6\text{-}f^5$ near the Fermi edge. In addition, there is a second part at the lower energy ($f^5\text{-}f^4$) which are more itinerant-like and merged into the quasi-particle subband [6]. Co-existence of these two types of the Hubbard bands in SmB_6 and PuB_6 defines them as Racah materials.

-
- [1] Khomskii, D. Mixed-valence problem. *Sov. Phys. Uspekhi* **22**, 879 (1979).
 - [2] Lawrence, J. M., Riseborough, P. S. & Parks, R. D. Valence fluctuation phenomena. *Rep. Prog. Phys.* **44**, 1 (1981).
 - [3] Johansson, B. Nature of the 5f electrons in the actinide series. *Phys. Rev. B* **11**, 2740 (1975).
 - [4] Katsnelson, M. I., Solovyev, I. V. & Trefilov, A. V. $\alpha - \delta$ transition in plutonium as a mott transition in an f - subsystem. *JETP Letters* **56**, 276 (1992).
 - [5] Colarieti-Tosti, M. *et al.* First-principles theory of intermediate-valence f-electron systems. *Phys. Rev. Lett.* **93**, 096403 (2004).
 - [6] Hanzawa, K. Theory of intermediate-valence states in Sm compounds. *J. Phys. Soc. Jpn.* **67**, 3151 (1998).
 - [7] Shick, A. B. *et al.* Unified character of correlation effects in unconventional Pu-based superconductors and δ -Pu. *Phys. Rev. B* **87**, 020505(R) (2013).
 - [8] Dzero, M., Sun, K., Galitski, V. & Coleman, P. Topological Kondo insulators. *Phys. Rev. Lett.* **104**, 106408 (2010).
 - [9] Lu, F., Jianzhou, Z., Hongming, W., Zhong, F. & Dai, X. Correlated topological insulators with mixed valence. *Phys. Rev. Lett.* **110**, 096401 (2013).
 - [10] Deng, X., Haule, K. & Kotliar, G. Plutonium Hexaboride is a correlated topological insulator. *Phys. Rev. Lett.* **111**, 176404 (2013).
 - [11] Weng, H., Zhao, Z., J. Wang, Fang, Z. & Dai, X. Topological crystalline Kondo insulator in mixed valence Ytterbium Borides. *Phys. Rev. Lett.* **112**, 016403 (2012).
 - [12] Smith, J. L. & Fisk, Z. Magnetism in transuranics. *J. Appl. Phys.* **53**, 7883 (1982).
 - [13] Shim, J. H., Haule, K. & Kotliar, G. Fluctuating valence in a correlated solid and the anomalous properties of delta-plutonium. *Nature* **446**, 513 (2007).
 - [14] Wachter, P. *in: Handbook on the Physics and Chemistry of the Rare Earths*, vol. 19 (Elsevier, Amsterdam, 1994).
 - [15] Denlinger, J. D. *et al.* SmB_6 Photoemission: Past and present arXiv:1312.6636 (unpublished).
 - [16] Denlinger, J. D. *et al.* Temperature dependence of linked gap and surface state evolution in the mixed valent topological insulator SmB_6 arXiv:1312.6637 (unpublished).
 - [17] Jiang, J. *et al.* Observation of possible topological in-gap surface states in the Kondo insulator SmB_6 by photoemission. *Nat. Commun.* **4**, 3010 (2013).
 - [18] Lichtenstein, A. I. & Katsnelson, M. I. *Phys. Rev. B* **57**, 6884 (1998).
 - [19] Hewson, A. *The Kondo Problem to Heavy Fermions* (Cambridge University Press, 1993).
 - [20] Kolorenc, J., Poteryaev, A. & Lichtenstein, A. I. Valence-band satellite in ferromagnetic nickel: LDA + DMFT study with exact diagonalization. *Phys. Rev. B* **85**, 235136 (2012).
 - [21] Shick, A. B., Kolorenc, J., Lichtenstein, A. I. & Havela, L. Electronic structure and spectral properties of Am, Cm, and Bk: Charge-density self-consistent LDA+HIA calculations in the FP-LAPW basis. *Phys. Rev. B* **80**, 085106 (2009).
 - [22] Shick, A. B., Lichtenstein, A. I. & Pickett, W. E. Implementation of the LDA+U method using the full-potential linearized augmented plane-wave basis. *Phys. Rev. B* **60**, 10763 (1999).
 - [23] Shick, A. B. & Pickett, W. Magnetism, spin-orbit coupling, and superconducting pairing in UGe_2 . *Phys. Rev. Lett.* **86**, 300 (2001).
 - [24] van der Marel, D. & Sawatzky, G. Electron-electron interaction and localization in d and f transition metals. *Phys. Rev. B* **37**, 10674 (1988).
 - [25] Lebegue, S., Svane, A., Lichtenstein, A. I., Katsnelson, M. I. & Eriksson, O. Multiplet effects in the electronic structure of light rare-earth metals. *Phys. Rev. B* **74**, 045114 (2006).
 - [26] Moore, K. & van der Laan, G. Nature of the 5f states in actinide metals. *Rev. Mod. Phys.* **81**, 235 (2009).
 - [27] Gunnarsson, O., Andersen, O. K., Jepsen, O. & Zaanen, J. Density-functional calculation of the parameters in the Anderson model: application to Mn in CdTe. *Phys. Rev. B* **39**, 1708 (1989).
 - [28] Roebler, S. *et al.* Hybridization gap and Fano resonance in SmB_6 . *PNAS* **111**, 4798 (2012).
 - [29] Chazalviel, J. N., Campagna, M., Wertheim, G. K. & Schmidt, P. H. Study of valence mixing in SmB_6 by x-ray

- photoelectron spectroscopy. *Phys. Rev. B* **14**, 4586 (1976).
- [30] Thunstrom, P. *et al.* Multiplet effects in the electronic structure of intermediate-valence compounds. *Phys. Rev. B* **79**, 165104 (2009).
 - [31] Racah, G. Theory of complex spectra. IV. *Phys. Rev.* **76**, 1352 (1949).
 - [32] Irkhin, V. Y. & Katsnelson, M. I. Theory of intermediate-valence semiconductors. *Sov. Phys. JETP* **63**, 631 (1986).
 - [33] Kikoin, K. A. Nature of the golden phase of Samarium monosulfide. *Sov. Phys. JETP* **85**, 1000 (1983).
 - [34] Altshuler, T. S., Mironov, V., Khaliulin, G. G. & Khomskii, D.. Observation of the temperature-dependence of the energy-gap in SmB₆ by the electron-paramagnetic-res method. *JETP Letters* **40**, 754 (1984).
 - [35] Gouder, T., Wastin, F., Rebizant, J. & Havela, L. 5f-electron localization in PuSe and PuSb. *Phys Rev. Lett.* **84**, 3378 (2000).
 - [36] Durakiewicz, T. *et al.* Electronic structure of actinide antimonides and tellurides from photoelectron spectroscopy. *Phys. Rev. B* **70**, 205103 (2004).
 - [37] Ichas, V., Griveau, J. C., Rebizant & Spirlet, J. C. High-pressure resistance of PuTe up to 25 GPa. *Phys. Rev. B* **63**, 045109 (2001).
 - [38] Yee, Ch. H., Kotliar, G., & Haule, K. Valence fluctuations and quasiparticle multiplets in plutonium chalcogenides and pnictides. *Phys. Rev. B* **81**, 035105 (2010).

ACKNOWLEDGEMENTS

The support from the Czech Republic grant GACR No. 15-07172S is acknowledged. AIL acknowledges financial support by Grant No. DFG LI 1413/8-1. MIK acknowledges financial support by ERC Advanced Grant No. 338957 and by NWO via Spinoza Prize.

AUTHOR CONTRIBUTIONS

ABS, MIK and AIL conceived and supervised the project. ABS and MIK performed the computations. All authors contributed to the interpretation of the data and to the writing of the manuscript.

ADDITIONAL INFORMATION

Competing financial interests: The authors declare no competing financial interests.

Supplementary Information for
Racah materials: role of atomic multiplets in intermediate valence systems

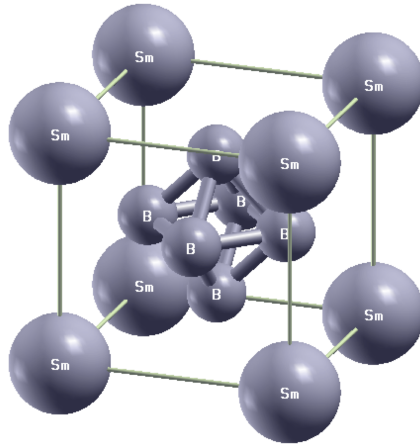
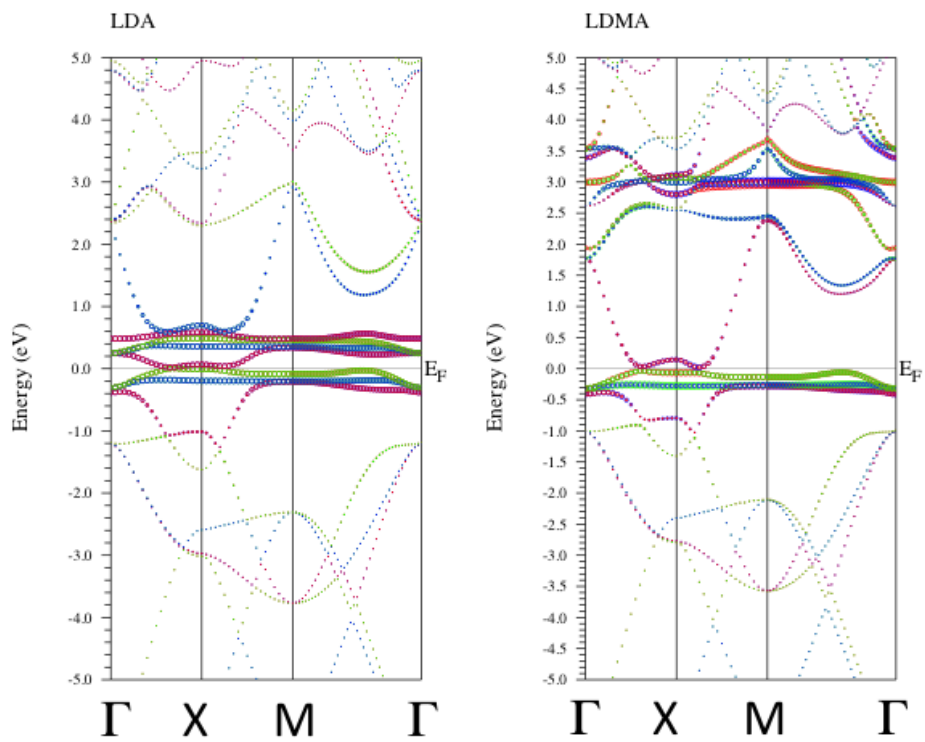


FIG. S1: The crystal structure of SmB₆.

SmB₆



PuB₆

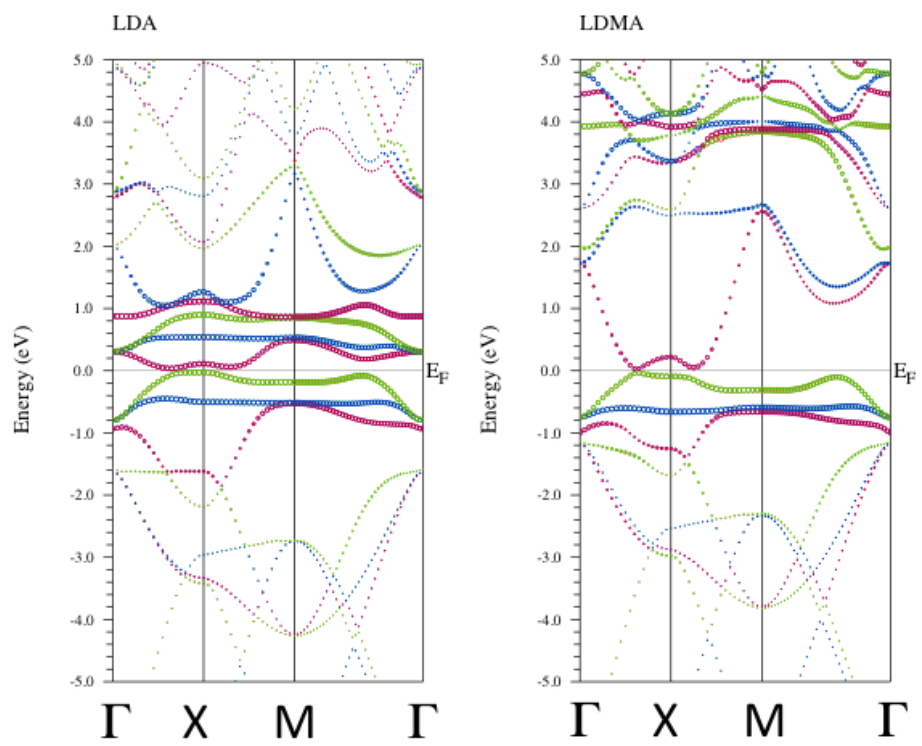


FIG. S2: SmB₆ (top) and PuB₆ (bottom) LDA and LDMA band structure.

In order to incorporate the dynamical self-energy effects into the LDMA band structure shown in Fig. 3 and Fig. S2, we make use of the first-order perturbation theory for the Green's function of the Eq. (3) with respect to $[\Sigma(z) - V_U]$, and write the \mathbf{k} -resolved spectral density $A(\mathbf{k}, z)$ as,

$$A(\mathbf{k}, z) = -\frac{Im}{\pi} \sum_n \left[\frac{1}{z + \mu - \epsilon_{\mathbf{k}}^n} + \frac{\langle \Phi_{\mathbf{k}}^n | \Sigma(z) - V_U | \Phi_{\mathbf{k}}^n \rangle}{(z + \mu - \epsilon_{\mathbf{k}}^n)^2} \right]. \quad (\text{S1})$$

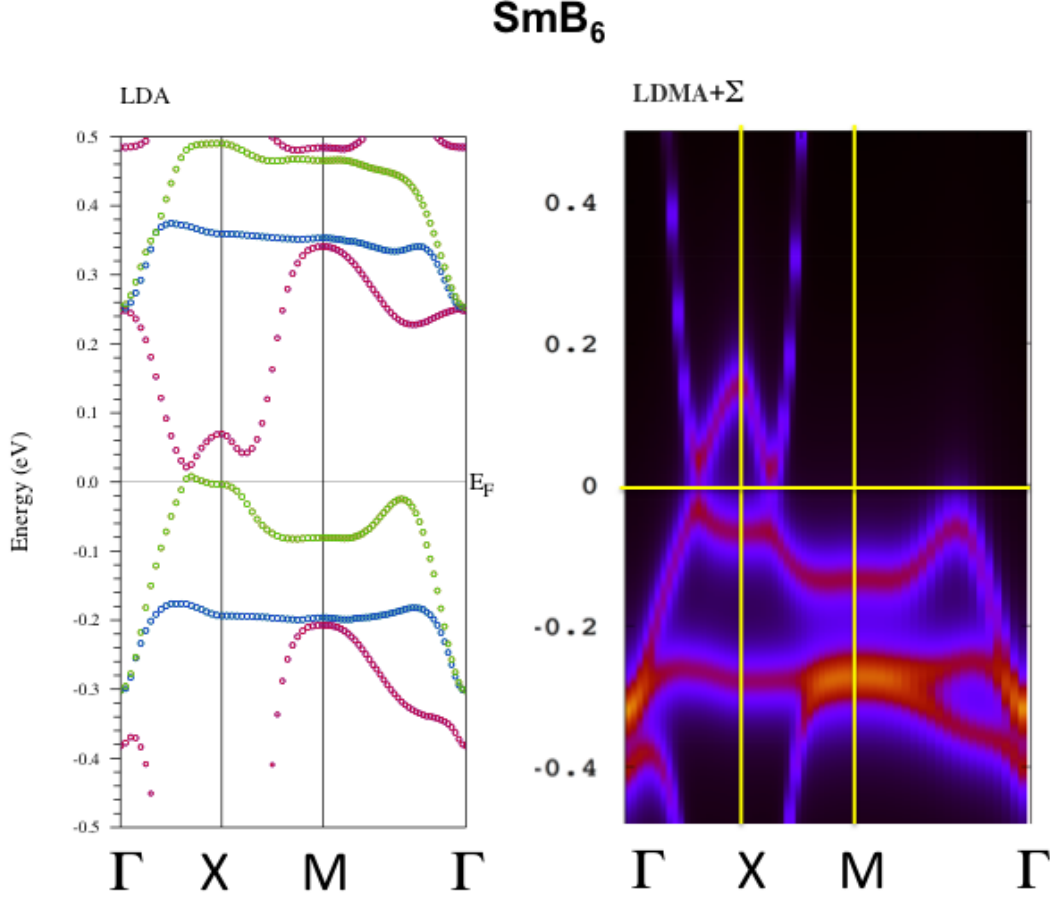


FIG. S3: SmB_6 LDA and LDMA + Σ band structure.

We plot the spectral density in Fig. S3 together with the LDA band structure for SmB_6 . We notice that the effect of $\Sigma(z)$ on the LDMA band structure shown in Fig. 3(top) is rather small. The indirect band gap is somewhat reduced to 30 meV becoming closer to the experimental value of 20 meV. Also, it resembles some features of the DMFT calculated spectral DOS [1] as well as the experimental angular resolved photoemission (ARPES) [2]. Since the experimental ARPES is known to be very surface sensitive, careful comparison with the theoretical calculations including the surface calculations is needed. These studies are beyond the scope of the present work, and left for the future.

[1] Junwon Kim *et al.*, Phys. Rev. B **90**, 075131 (2014).

[2] J. D. Denlinger *et al.*, JPS Conf. Proc. **3**, 017038 (2014).